

E9-2009-192

D. Dinev*

REVIEW OF COHERENT INSTABILITIES
IN SYNCHROTRONS AND STORAGE RINGS

*Institute for Nuclear Research and Nuclear Energy, 72 Tzarigradsko
Shaussee Blvd., Sofia-1784, Bulgaria

Динев Д.
Обзор когерентных неустойчивостей
в синхротронах и накопительных кольцах

E9-2009-192

Когерентные неустойчивости являются одним из основных факторов, ограничивающих эксплуатационные качества пучков в синхротронах и накопительных кольцах. В обзоре рассматриваются как продольные, так и поперечные неустойчивости. Обсуждаются неустойчивости в непрерывных и сбанчированных пучках при низкой и высокой интенсивности. В обзоре приводится информация для практического применения при проектировании ускорителей.

Работа выполнена в Лаборатории физики высоких энергий им. В. И. Векслера и А. М. Балдина ОИЯИ.

Сообщение Объединенного института ядерных исследований. Дубна, 2009

Dinev D.
Review of Coherent Instabilities
in Synchrotrons and Storage Rings

E9-2009-192

Coherent instabilities are one of the main factors limiting the performance of synchrotrons and storage rings. Both longitudinal and transverse instabilities are reviewed. Instabilities in coasting and bunched beams at low and high intensity are discussed. The paper is purposed for practical usage while accelerator design.

The investigation has been performed at the Veksler and Baldin Laboratory of High Energy Physics, JINR.

Communication of the Joint Institute for Nuclear Research. Dubna, 2009

1. IMPEDANCES AND WAKE FIELDS

Charged particles accelerated in a circular accelerator are a source of EM fields that act back on the beam perturbing the motion. This may cause dangerous feedbacks leading to different kinds of instabilities — Fig. 1.

The self-fields are a superposition of EM field generated by the beam in the free space and of EM field produced by the image current induced on the vacuum chamber walls. The wall geometry is complicated. The smooth metallic (usually stainless steel) vacuum pipe with an oval cross section is interrupted by steps, BPM plates, RF cavities, bellows, flanges, ferrite kickers, septum magnets, etc. The EM field produced by the beam and modified by the beam surroundings causes a force that acts back on the particles. Together with the force due to the external EM fields, which imposes the particle trajectories, this self-force affects the motion of the particles in the accelerator, and under some circumstances this motion becomes unstable.

It is impossible to solve analytically Maxwell's equations taking into account a very complicated geometry of the vacuum chamber and various electromagnetic properties of the walls. In an effort to generalize all the cases of wall geometry, V.C. Vaccaro and A.M. Sessler have introduced the concept of wake fields and impedances [1–5].

The coupling impedance gathers in one quantity all the details of the electromagnetic interaction of the beam and its surroundings. The longitudinal impedance is defined by one-turn voltage seen by the particles:

$$E_z(t, \theta) = -\frac{1}{2\pi R} Z_{\square}(\omega) I(t, \theta), \quad (1)$$

where θ is the azimuth, R is the machine mean radius, E_z is the longitudinal electric field, and I is the beam current.

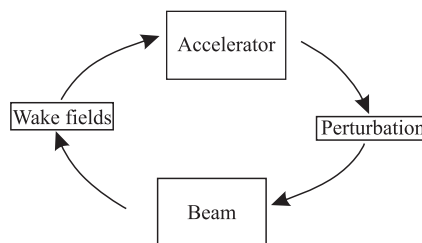


Fig. 1. The beam-environment feedback may lead to instability

Introducing the Fourier components of the beam current we have:

$$E_z(t, \theta) = -\frac{1}{2\pi R} \int_{-\infty}^{\infty} Z_{\square}(\omega) I(\omega, \theta) e^{i\omega t} d\omega. \quad (2)$$

The transverse signal as it is measured by the PUEs, is defined as the product of the beam current by the local center-of-mass displacement $\langle x \rangle$:

$$D(t, \theta) = I(t, \theta) \langle x(\theta) \rangle. \quad (3)$$

By historical reasons, the transverse coupling impedance is defined as:

$$[\vec{E} + \vec{\beta}c \times \vec{B}]_{\perp}(t, \theta) = -\frac{i\beta_0}{2\pi R} \int_{-\infty}^{\infty} Z_{\perp}(\omega) D(\omega, \theta) e^{i\omega t} d\omega, \quad (4)$$

i. e., the transverse deflecting force on the unit charge (Lorentz force) over one particle revolution divided by the dipole moment of the beam.

The dimension of Z_{\parallel} is $[\Omega]$ and of Z_{\perp} is $[\Omega/m]$. The impedance is a complex function of frequency.

Types of the beam environment can be classified in the following way.

- *Perfectly conducting walls of uniform cross section (case of space-charge dominated beam)*. The EM field emitted by an ultrarelativistic particle moving with a velocity βc in a smooth pipe with perfectly conducting walls, is purely transverse:

$$\begin{aligned} E_r &= \frac{1}{2\pi\epsilon_0 r} \delta(z - \beta ct), \\ H_{\phi} &= \frac{1}{2\pi Z_0 r} \delta(z - \beta ct), \end{aligned} \quad (5)$$

where

$$Z_0 = \sqrt{\frac{\mu_0}{\epsilon_0}} = 376.7 \Omega \quad (6)$$

is the free-space impedance,

In the limit $\beta \rightarrow \infty$, the field is as in the free space. This «pancake»-like field will not act on the particles moving in front of or behind the source particle — Fig. 2.

In the longitudinal direction, the coupling impedance is (see Fig. 3):

$$Z_{\square}^{SC}(\omega) = -\frac{i Z_0 g}{2\beta_0 \gamma_0^2} \frac{\omega}{\omega_0}, \quad (7)$$

$$g = 1 + 2 \ln\left(\frac{b}{a}\right), \quad (8)$$

where a is the beam radius, b is the vacuum chamber radius.

The space-charge impedance is purely reactive (negative inductance), i.e., there is no energy loss during the particle motion.

In the transverse direction:

$$Z_{\perp}^{SC}(\omega) = -\frac{i R Z_0}{\beta_0^2 \gamma_0^2} \left(\frac{1}{a^2} - \frac{1}{b^2} \right). \quad (9)$$

The transverse space-charge impedance is shown in Fig. 4.

The lower the particle energy is the higher the space-charge impedance.

• *Walls with finite conductivity σ .* In the realistic case of the walls with finite conductivity σ , when the wall thickness is greater than the skin depth δ :

$$\delta = \sqrt{\frac{2}{\mu \sigma \omega}}, \quad (10)$$

the EM field emitted by the source particle is more complicated — Fig. 5.

At the distances bigger than d_0 behind the source particle, the EM field is accelerating the trailing particles of the same charge sign, while at the distances less than d_0 , it is decelerating in agreement with the energy balance condition

$$d_0 = \sqrt[3]{\frac{b^2}{Z_0 \sigma}}. \quad (11)$$

In the longitudinal direction, the coupling impedance is (see Fig. 6):

$$Z_{\square}^{RW}(\omega) = (1 + i) \frac{Z_0 \beta_0 \delta \omega}{2b \omega_0}. \quad (12)$$

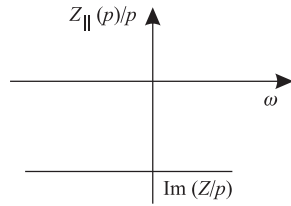


Fig. 3. Longitudinal space-charge impedance $Z_{\square}(p)/p$, $p = \omega/\omega_0$

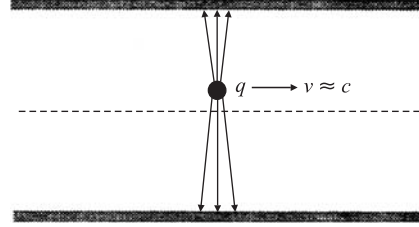


Fig. 2. EM field of the ultrarelativistic charge moving in a perfectly conducting pipe

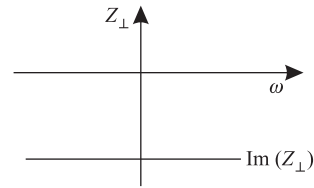


Fig. 4. Transverse space-charge impedance Z_{\perp}

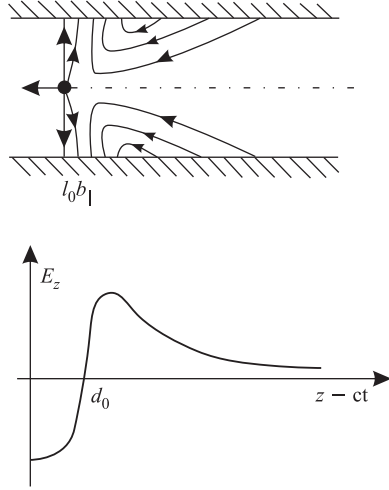


Fig. 5. EM field in the vacuum pipe with finite conductivity

fundamental mode, at frequency $\omega_{RF} = h\omega_0$ the accelerating cavities have many other sharp resonances corresponding to all the resonant modes of the RF structure (higher-order modes, HOMs). When a bunch passes through the cavity, it could excite these parasitic modes.

The field in the resonant element decays as $\exp(-\frac{\omega_r}{2Q}t)$, where ω_r is the resonance frequency, and Q is the quality factor. Time $t = 2Q/\omega_r$ is needed for the excited field to reduce «e» times. As in the RF cavities the quality factor Q is very high, 10^4 or higher, this field lasts long enough to couple the successive bunches circulating around the ring.

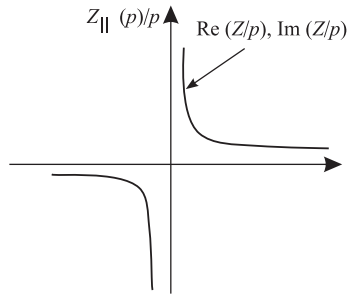


Fig. 6. Longitudinal resistive wall impedance

In the transverse direction, the coupling impedance could be calculated applying the relation between the transverse and longitudinal impedances:

$$Z_{\perp} = \frac{2c}{b^2} \frac{Z_{\square}}{\omega}, \quad (13)$$

$$Z_{\perp}^{RW} r = (1 + i) \frac{R Z_0}{b^3} \delta. \quad (14)$$

Due to the factor b^3 in the denominator, accelerators with a small cross section of the vacuum chamber have large resistive wall impedance.

The transverse resistive wall impedance is shown in Fig. 7.

• *Resonant element.* The EM fields generated by the beam in the RF cavities are between the main sources of beam-environmental interactions. Instead of the

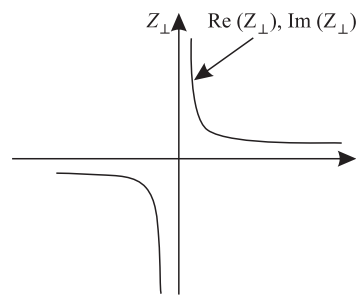


Fig. 7. Transverse resistive wall impedance

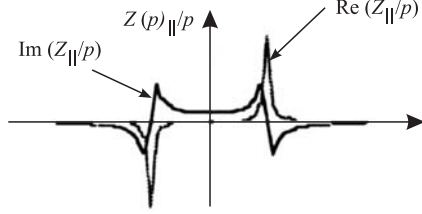


Fig. 8. Longitudinal narrow-band resonant impedance

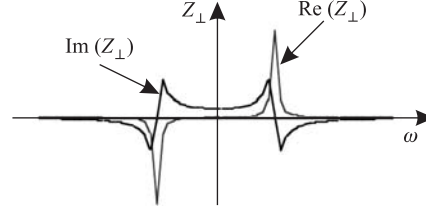


Fig. 9. Transverse narrow-band resonant impedance

The longitudinal coupling impedance of a resonator is:

$$Z_{\square} = \frac{R_s}{1 + iQ \left(\frac{\omega}{\omega_r} - \frac{\omega_r}{\omega} \right)}, \quad (15)$$

where R_s is the shunt impedance of the resonator.

Below resonant frequency ($\omega \ll \omega_r$) the impedance is pure inductance; at resonance ($\omega = \omega_r$) is pure resistance, and above transition ($\omega \gg \omega_r$) is pure capacitance. The bandwidth (HWHM) is:

$$\delta\omega = \frac{\omega_r}{2Q}. \quad (16)$$

The longitudinal narrow-band resonant impedance is shown in Fig. 8.

If in the accelerator there are many bunches, the attenuation between two successive bunches is given by $\exp(-\alpha)$, where:

$$\alpha = \pi \frac{f_r t_{\text{bunch-bunch}}}{Q}. \quad (17)$$

In the case of high Q (narrow band) resonator, the decay of the wake field is slow ($\alpha \ll 1$). Such a long-range wake field is a source of bunch coupling. The wake field of a narrow-band resonator lasts for a long period of time, and successive bunches will be coupled by such resonator.

The transverse narrow-band resonant impedance is shown in Fig. 9.

• *Broad-band (BB) resonant element.* This is the case of low quality factor ($Q \sim 1$) and high attenuation of the field ($\alpha \gg 1$). Changes of vacuum chamber such as bellows, flanges, etc., can trap some magnetic field. The measurements on many existing machines have shown that such structures are well approximated by a BB resonator with $Q \sim 1$, and resonant frequency around the vacuum chamber pipe cut-off frequency (~ 1 GHz) is

$$\omega_r \approx \omega_{c.o.} = \frac{c}{b}. \quad (18)$$

The shunt impedance of this BB resonator is adjusted to fit the impedance observed at low frequencies. Just at resonance we have pure resistance $Z(\omega_r) = R_{sh}$. The BB resonator has an impedance curve with a large bandwidth ($\frac{1}{\delta f} \gg \frac{T_0}{M}$), M is the number of bunches and therefore the wake field decays rapidly. This element represents local interactions which can couple only close particles. The longitudinal broad-band resonant impedance is shown in Fig. 10.

The transverse broad-band resonant impedance is shown in Fig. 11. Let us consider two-point charges rotating in a circular accelerator at frequency $\omega_0 = \beta_0 c/R$. The leading particle has charge q Coulombs. Following τ seconds behind is a unit charge. Let $E_z(z, t)$ be the longitudinal component of the electric field generated by the leading particle.

The longitudinal wake potential (function) is defined as the potential per unit charge seen by the trailing particle:

$$w_{\square}(\tau) = -\frac{1}{q} \int_{-\infty}^{\infty} E_z(z, \frac{z}{\beta c} + \tau) dz. \quad (19)$$

The dimension of wake potential is $[\Omega/s]$. This is a real function of time.

It could be shown that the wake potential is a Fourier transfer of the coupling impedance:

$$w_{\parallel}(\tau) = \frac{1}{2\pi} \int_{-\infty}^{\infty} Z_{\parallel}(\omega) e^{i\omega\tau} d\omega. \quad (20)$$

For smooth enough impedance or a long enough machine so that the wake field is equal to zero after one revolution, it could be proved that:

$$w_{\parallel}(\tau) \approx -\frac{2\pi R}{q} E_z(\tau), \quad (21)$$

i.e., the wake potential is equal to one-turn voltage seen by the trailing particle per unit charge.

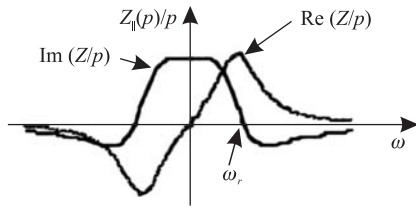


Fig. 10. Longitudinal broad-band resonant impedance

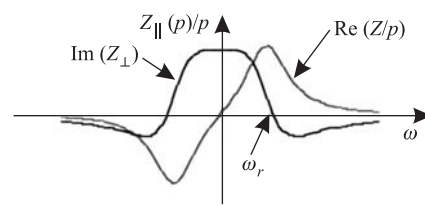


Fig. 11. Transverse broad-band resonant impedance

When the source and the test particles move not just on the axes but on parallel to their trajectories, the test particle will experience also a transverse force. The transverse wake potential is defined as follows:

$$w_{\perp}(\tau) = -\frac{1}{q} \int_{-\infty}^{\infty} [\vec{E} + \vec{\beta}c \times \vec{B}]_{\perp}(z, \frac{z}{\beta c} + \tau) dz. \quad (22)$$

The EM fields generated by the source particle fall in two categories. The long-range wake fields decay so slowly that can affect the particles in the next bunches. The short-range wakes decay fast and they provide influence between the particles of the same bunch but have no effect on the other bunches.

Useful formula for coupling impedances and wake functions are given in Appendix 1, taken from [B3].

2. COASTING BEAM COHERENT INSTABILITIES [6-9]

2.1. Longitudinal Direction. Coasting beam is a beam of particles uniformly distributed around the accelerator circumference — Fig. 12.

On the stationary signal I , a perturbation in the form of travelling waves with « p » wavelength around the ring, is superimposed — Fig. 13. In a frame moving with the synchronous particle (angular velocity ω_0), the azimuth of the test particle relative to the synchronous particle is $\Delta\theta$. The travelling wave in this coordinate system will be:

$$\hat{I}_p e^{i(\omega_{\parallel PC} t - p\Delta\theta)}. \quad (23)$$

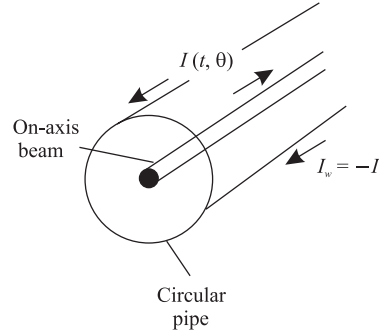


Fig. 12. Coasting beam and wall currents

In the stationary laboratory system this wave will be:

$$\hat{I}_p e^{i(\Omega_c t - p\theta)}, \quad \Omega_c = p\omega_0 + \omega_{\parallel PC}. \quad (24)$$

Our patten consists in a closed wave of linear particle density with p wavelengths along the accelerator circumference. The angular phase velocity of the wave in the moving frame is $\omega_{\square PC}/p$ while in the laboratory frame it is $\Omega_c/p = \omega_0 + \omega_{\square PC}/p$.

In the time domain

$$I(t, \theta) = I + \hat{I}_p e^{i(\Omega_c t - p\theta)}, \quad (25)$$

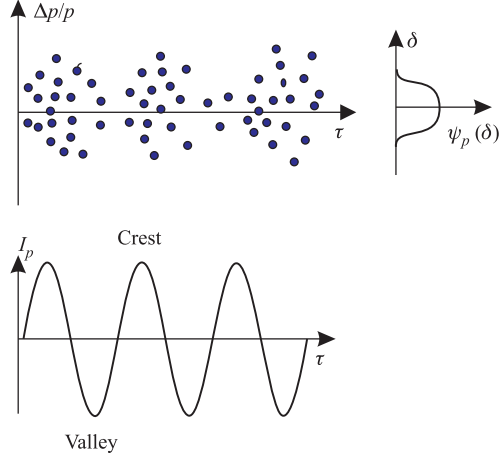


Fig. 13. Longitudinal perturbation

where

$$I = \frac{eZN\beta c}{2\pi R} \quad (26)$$

is the average current.

In the frequency domain:

$$I(\omega, \theta) = I \delta(\omega) + \hat{I}_p e^{-ip\theta} \delta(\omega - \Omega_c), \quad (27)$$

i.e., the spectrum consists of two lines at $\omega = 0$ and at $\omega = \Omega_c$.

If

$$Im(\omega_{\square pc}) < 0, \quad (28)$$

the perturbation will increase exponentially with the time and the beam gets bunched at harmonic « p » — Fig. 13. The growth rate of the instability is:

$$\frac{1}{\tau_i} = -Im(\omega_{\square pc}). \quad (29)$$

The coherent instabilities prevent the beam current from being increased above the certain threshold. This kind of instability leads to an increase of the momentum spread.

The dispersion relation from which $\omega_{\square PC}$ can be revealed, is obtained applying Vlasov's equation. We will not go in further details but only summarize the final results.

1. For a monochromatic beam:

- In the case of space-charge dominated interaction, the beam is stable below transition ($\eta < 0$) and unstable above transition ($\eta > 0$) — negative-mass instability.
- For the practically important case of BB impedance at low frequencies, the above result is inverted.
- If the beam is cold and some resistance is present, the line density modulation will grow up and instability will take place.

2. For a coasting beam with momentum spread, the motion is stabilized by the Landau damping mechanism. Landau damping is a phenomenon well known from plasma physics. This is a natural mechanism that stabilizes the coherent instabilities. In the presence of frequency spread, a collection of lossless oscillators responds like a damped oscillator. In the transverse direction, the spread in the betatron tune is due to different energies of the particles in the beam and to the nonlinearities in the magnetic field which cause the dependence of frequency on the amplitude. In the longitudinal direction, the spread in the synchrotron tune is due to the nonlinear character of the RF voltage. Also the revolution frequency depends on the particle energy. The stability criterion is given by the Keil-Schnell formula [10, 11]:

$$\left| \frac{Z_{\parallel}(p)}{p} \right| \leq \frac{\left(\frac{m_0 c^2}{e} \right) |\eta| \gamma_0 \beta_0^2}{\left(\frac{q}{A} I \right)} \left(\frac{\Delta p}{p} \right)_{FWHM}. \quad (30)$$

2.2. Transverse Direction. In the transverse plane, the perturbation consists of a slight initial displacement of the beam in the transverse direction — Fig. 14. This causes coherent oscillations of the particles in the external focusing field.

In the time domain, the wave of the coherent betatron oscillation is:

$$D(t, \theta) = \hat{D} e^{i[(p\omega_0 + \omega_{\perp PC})t - p\theta]}, \quad (31)$$

in the frequency domain:

$$D(\omega, \theta) = \hat{D} e^{-ip\theta} \delta[\omega - (p\omega_0 + \omega_{\perp PC})]. \quad (32)$$

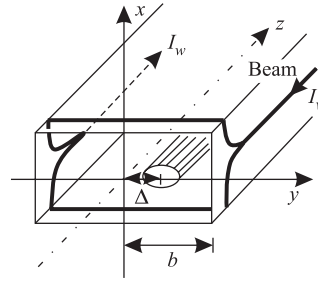


Fig. 14. Transverse instability

The dispersion relation has two roots — lower and upper betatron sidebands:

$$\omega_{\perp pc}^- = Q_{pc}^- \omega_0 = -(Q_0 + \Delta Q_{pc}) \omega_0, \quad (33)$$

$$\omega_{\perp pc}^+ = Q_{pc}^+ \omega_0 = (Q_0 + \Delta Q_{pc}) \omega_0, \quad (34)$$

where ΔQ_{PC} is the coherent transverse betatron tune shift.

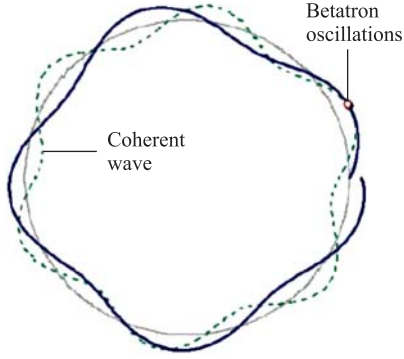


Fig. 15. Waves in a coasting beam

For «-» solution the angular phase velocity of the coherent wave is less than the angular beam velocity ω_0 :

$$\omega_{ph}^- = \omega_0 - \frac{(Q_0 + \Delta Q_{pc})}{p}. \quad (35)$$

For that reason it is called the slow wave.

For «+» solution the angular phase velocity of the coherent wave is greater than the angular beam velocity:

$$\omega_{ph}^+ = \omega_0 + \frac{(Q_0 + \Delta Q_{pc})}{p}, \quad (36)$$

and is called the fast wave — Fig. 15.

So, in the time domain the slow and fast waves have the following forms:

$$D^-(t, \theta) = \hat{D} e^{i[(p-Q_0)\omega_0 t - p\theta]} e^{-i\Delta Q_{pc}\omega_0 t}, \quad (37)$$

$$D^+(t, \theta) = \hat{D} e^{i[(p+Q_0)\omega_0 t - p\theta]} e^{i\Delta Q_{pc}\omega_0 t}. \quad (38)$$

The transverse spectrum consists of the lower and upper betatron sidebands around harmonics of the revolution frequency:

$$D^-(\omega, \theta) = \hat{D} e^{-ip\theta} \delta[\omega - (p - Q_0 - \Delta Q_{pc})\omega_0], \quad (39)$$

$$D^+(\omega, \theta) = \hat{D} e^{-ip\theta} \delta[\omega - (p + Q_0 + \Delta Q_{pc})\omega_0]. \quad (40)$$

The stability of the motion is determined by $Im(\Delta Q_{pc})$.

For the cold beam (beam without tune spread) if the impedance has a resistive part, the fast wave is always stable and the slow wave is always unstable. If Z_\perp is purely imaginary, the motion will be stable and the frequency shift $\omega_{\perp pc}$ will be a real number.

The momentum spread in the beam can stabilize the motion through the Landau damping mechanism. The criterion for the transverse stability is given by the following equation:

$$|Z_\perp((p - Q_0)\omega_0)| \leq \frac{4Q_0 \left(\frac{m_0 c^2}{e}\right) \gamma_0}{\left(\frac{q}{A}\right) I c} [(p - Q_0)\omega_0 + \omega_\xi] \eta \left(\frac{\Delta p}{p}\right)_{FWHM}, \quad (41)$$

where η is the frequency slip factor, ξ is the chromaticity, ω_ξ — betatron angular frequency shift due to chromaticity:

$$\omega_\xi = Q_0 \omega_0 \frac{\xi}{\eta}. \quad (42)$$

3. BUNCHED BEAM COHERENT INSTABILITIES [12, 13]

3.1. Longitudinal Direction. The longitudinal instabilities can be looked at from different viewpoints.

From the point of view how fast instabilities develop in time, they are divided into two categories:

1. *Slow instabilities*: $\tau_i > T_s$, where τ_i is the instability rise time, and T_s is the period of synchrotron oscillations.
2. *Fast instabilities*: $T_s > \tau_i > T_0$, where T_0 is the revolution period of time.

From the point of view of the perturbation range:

1. *Instabilities with short wavelength*: $\lambda_p < \sigma_L$, where λ_p is the wavelength of the perturbation, and σ_L is the rms bunch length in m .
2. *Instabilities with long wavelength*: $\lambda_p > \sigma_L$.

We have to separate also the cases of a single bunch from cases of multiple bunches.

I. *Single bunch longitudinal instabilities [14–18]*. If the beam-environment interaction is local (delta function wake), successive bunches ignore each other.

The single bunch stationary distribution in the longitudinal phase space depends only on the momentum (energy) deviations from the reference momentum (energy). The spectrum is linear at harmonics of the revolution frequency ($p\omega_0$). There are no synchrotron satellites; the synchrotron motion is hidden in the bunch. The spectrum is peaked at zero frequency and extends to $\pm 2\pi/\tau_L$, where τ_L is the full bunch length in s , 4σ for Gaussian bunches. The EM field induced by the stationary distribution is also at harmonics of revolution frequency.

The perturbation consists in small oscillations (in azimuth and in time) about the stationary distribution. The longitudinal perturbation introduces EM fields at harmonics of synchrotron frequency. The spectrum of the perturbation consists of lines at

$$\omega = p\omega_0 + m\omega_s + \Delta\omega_{cm}, \quad (43)$$

where $\Delta\omega_{cm}$ is the coherent frequency shift. This is a complex number. Its imaginary part determines whether the motion is stable or unstable. Instability occurs when

$$Im(\Delta\omega_{cm}) < 0. \quad (44)$$

The spectrum is peaked at

$$\frac{(m+1)\pi}{\tau_L}, \quad (45)$$

and extends to $\pm 2\pi/\tau_L$.

The type of oscillation of individual bunches is specified by the integer index m — the synchrotron mode. $m = 1$ denotes the so-called dipole mode, which represents off-centered oscillations of a rigid bunch in the longitudinal

phase space — Fig. 16. The coherent dipolar perturbation is caused by RF phase errors or energy errors. The dipole perturbation develops in time with a coherent frequency:

$$\omega_c = \omega_s + \Delta\omega_{c1}, \quad (46)$$

$m = 2$ denotes the quadrupole or breathing mode, which represents the bunch shape oscillations in the longitudinal phase space — Fig. 17. It is caused by RF focusing mismatched. The EM field induced by the quadrupole perturbation is at frequencies

$$p\omega_0 + 2\omega_s + \Delta\omega_{c2}. \quad (47)$$

The line density distribution of the first two longitudinal modes is shown in Fig. 18.

II. *Coupled bunch longitudinal instabilities [14-18].* Coupled bunch modes are dominated by the resonant impedance (narrow band). Such impedance is due to parasitic higher order modes in the RF cavities. In this case the attenuation of the wake field between two successive bunches is weak — the environment can memorize the passing of a bunch longer than the bunch repetition period. For M

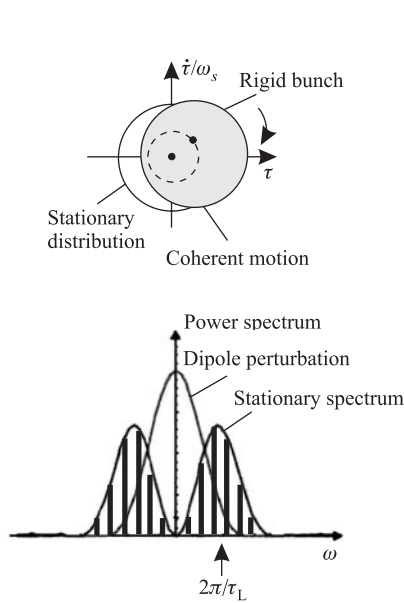


Fig. 16. Dipole (rigid) mode

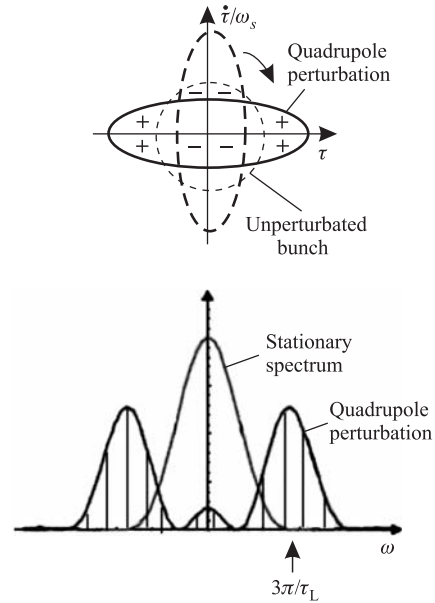


Fig. 17. Quadrupole (breathing) mode

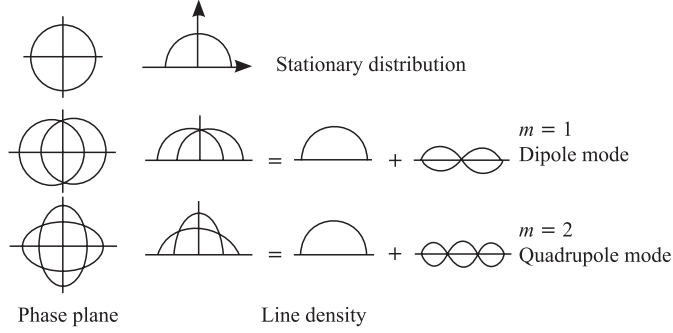


Fig. 18. Line density distribution of the first longitudinal modes

equally spaced bunches only every M^{th} line occurs in the spectrum:

$$\omega_p = (n + pM) \omega_0 + m \omega_s + \Delta\omega_{cm}, \quad (48)$$

where $n = 0, 1, \dots, (M - 1)$ is the so-called coupled-bunch mode number. It specifies how the individual bunch modes are lined together. The phase shift between oscillations in successive bunches is $2\pi n/M$. Another line of separation is between the low and high intensity cases.

3.1.1. Low Intensity Longitudinal Instabilities. Low intensity coherent modes are well described by F. Sachere's integral equation or J. Laclare's eigenvalue equation. A resistance is needed to drive the instability depending on the sign of the revolution harmonic number « p ». Below transition upper sidebands (positive « p ») are stable and lower sidebands (negative « p ») are unstable. Above transition the situation is reversed.

In the case of a single bunch or two bunches ($M = 1, 2$), the upper and lower sidebands in the spectrum belong to the same mode « n ». The impedance will cover both sidebands which will cancel each other. In the case of more than two bunches ($M \geq 2$), the upper and lower sidebands belong to different couple-bunch modes « n ». In this case even a resonator with a narrow band impedance curve will push up one of the couple-bunch modes and suppress the other.

For the couple-bunch mode it is needed to have the narrow band resonant impedance with impedance decay time much longer than the time between two successive bunches;

$$\frac{1}{\Gamma} \gg \frac{T_0}{M}, \quad (49)$$

where Γ is the width of $Z(\omega)$.

Let us now look how different types of longitudinal coupling impedances drive the couple-bunch instability.

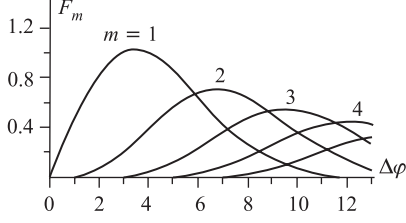


Fig. 19. Form factor

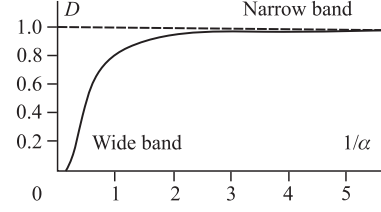


Fig. 20. Attenuation factor

— *Space-charge impedance.* In this case $iZ(p)/p$ is constant and real. There is no instability. The coherent frequency is real. Once started, the synchrotron mode « m » continues to oscillate infinitely.

— *Resistive wall impedance.* It is peaked at low frequencies and acts very weakly on the longitudinal motion and can be neglected.

— *Parasitic high Q modes in the RF cavities.* If the distance between two adjacent lines in the spectrum is larger than the resonator bandwidth $\Delta\omega$, a single line will drive the instability. For large bandwidths, more than one line must be taken into account and there is some cancellation between the upper and lower sidebands. The growth rate of the instability is:

$$\frac{1}{\tau_i} = -\text{Im}(\Delta\omega_{cm}) = \frac{m\omega_s}{m+1} \frac{4MI}{\pi^2 B^2 h V \cos \phi_s} \frac{R_s \omega_0}{\omega_r} F_m D, \quad (50)$$

where:

$$D = \frac{\alpha}{\sinh(\alpha)}, \quad (51)$$

$$\alpha = \frac{\pi \omega_r}{Q \omega_0 M}, \quad (52)$$

F_m is a form factor — Fig. 19, and D is an attenuation factor — Fig. 20. There is no instability for wake fields that decay appreciably before the next bunch to arrive.

3.1.1.1. Robinson's Instability. The RF cavities of a circular accelerator are tuned to the fundamental mode $\omega_r = h\omega_0$, h is the harmonic number. The quality factor Q is very high and the resonator bandwidth $\Delta\omega$ is very narrow.

In these circumstances, the imaginary part of the coherent frequency which indicates whether the motion will be stable or unstable, is proportional to the difference of the resonator resistance at the upper coherent sideband ($h\omega_0 + m\omega_s$) and at the lower coherent sideband ($h\omega_0 - m\omega_s$):

$$\text{Im}(\omega_c) \sim \frac{I}{V \cos \phi_s} [R(h\omega_0 + m\omega_s) - R(h\omega_0 - m\omega_s)]. \quad (53)$$

As below the transition $\cos \phi_s > 0$, the beam will be unstable ($Im(\omega_c) < 0$) if the resonant frequency ω_r is slightly below $h\omega_0$ — Fig. 21. Above the transition, the condition for instability is reversed.

The so-described phenomenon is known as Robinson's effect — [22].

Qualitatively, if $\Delta E > 0$ below transition, then $\Delta\omega > 0$ and the bunch will move to the right and see lower resistance R_- . Thus, less energy will be taken from the beam and ΔE will continue to increase, i. e., some instability will occur.

The Robinson instability is removed by tuning the RF cavity slightly away from $h\omega_0$ or recently by applying an active feedback.

3.1.2. High Intensity Longitudinal Instabilities. In the case of low intensity the coherent force is treated as a perturbation compared to the longitudinally focusing by RF cavities. In this case different synchrotron modes « m » are decoupled. This is the case of low beam intensity.

If the beam intensity is high, the spectra of synchrotron modes « m » and « $m + 1$ » will be very close and partly overlapped. While increasing the beam current, the bunch lengthening suddenly jumps up — this phenomenon is called turbulent bunch lengthening. Also the bunch widening or increasing of $\Delta p/p$ takes place. All these can be explained by synchrotron mode coupling.

3.1.2.1. Microwave Instability (MWI). This is the high-frequency-fast-single-bunch instability. The microwave instability develops in time with frequency $\Omega > \omega_s$, ω_s being the synchrotron frequency. Also the perturbation wavelength is much shorter than the bunch length: $\lambda_p < \sigma_L$. The PUE signal is in the microwave region, from 100 MHz up to several GHz. MWI has been observed for the first time in CERN PS and ISR [19, 20].

The microwave instability is observed in high intensity machines. This is a single bunch effect. It leads to a very fast blow-up of the bunch area which soon exceeds the longitudinal acceptance of the accelerator.

According to the suggestion by D. Boussard [19] the condition of the microwave instability is given by the coasting beam stability criterion by Keil and Schnell, but the local values of current and $\Delta p/p$ must be used instead of average current. This approach predicts the instability threshold quite well:

$$\left| \frac{Z_{\square}(p)}{p} \right| \leq \frac{2\pi |\eta| E_0 A}{qe I_{\text{peak}}} \left(\frac{\Delta p}{p} \right)^2, \quad (54)$$

$$|Z_{\perp}| \leq \frac{4\sqrt{2\pi} |\eta| E_0 A}{qe I_{\text{peak}} \langle \beta \rangle} \left(\frac{\Delta p}{p} \right). \quad (55)$$

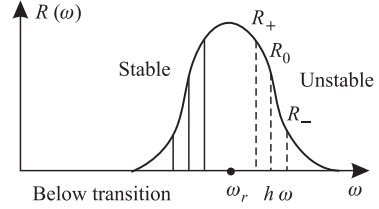


Fig. 21. Robinson instability

The peak current depends on the distribution of particles in the bunch or bunching factor. By definition:

$$B_f = \frac{I_0}{I_{\text{peak}}} \quad (56)$$

for M bunches in the ring:

$$B_f = \frac{ML}{S2\pi R}, \quad (57)$$

where L is the full bunch length, $L = 4\sigma_L$ for Gaussian bunch, and S is a shape factor, $S = 1$ — for «water bag» bunch, $S = 1.6$ — for a Gaussian bunch.

3.2. Transverse Direction. In the transverse direction a modulation of the betatron oscillations by synchrotron motion takes place. This is the source of the so-called head-tail modes.

The spectrum of the transverse perturbation is a line spectrum at frequencies $\omega = (p + Q)\omega_0 + m\omega_s$, $p = \dots, -1, 0, +1, \dots$ and $m = 0, 1, 2, \dots$. Synchrotron modes « m » are no longer sidebands of the revolution harmonics $p\omega_0$. They are now sidebands of the betatron sidebands, the upper: $(p + Q)\omega_0$ and lower: $(p - Q)\omega_0$. The transverse perturbation is coherent only with the synchrotron satellite number « m »

$$D(\omega, \theta) = \frac{4\pi^2 I}{2} \sum_{p=-\infty}^{\infty} e^{-ip\theta} \sigma_m(p) \delta(\omega - [(p + Q)\omega_0 + m\omega_s + \Delta\omega_{cm}]). \quad (58)$$

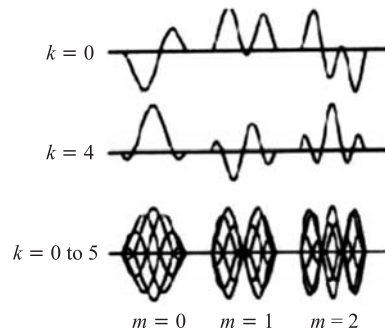


Fig. 22. Transverse PUE signals for the low order coherent modes. The revolution number is denoted by k . Five passages of the beam are superimposed at the third line

The transverse PUE signals for the first three coherent modes are shown in Fig. 22.

It is essential that the spectrum is centered at ω_ξ — the betatron frequency shift due to chromaticity. This is the fundamental difference between the transverse and the longitudinal cases. For standard machines the uncorrected chromaticity ξ is negative, therefore ω_ξ is a negative frequency above the transition energy and positive frequency below this.

The mechanism of the head-tail instability is shown in Fig. 23.

Particles at the head of the bunch generate transverse wake fields that will excite oscillations of the particles at the bunch tail.

Because of the synchrotron motion after a half synchrotron period, the tail particles will go to the bunch head and vice versa. New transverse wakes are generated that affects the new tail particles.

If the head-tail particle exchange and the excitation by the transverse wake fields act in the phase, the particle oscillations will grow up and instability will happen.

A photo of the first three head-tail modes registered at CERN PSB is shown in Fig. 24. If the transverse impedance is sufficiently smooth, the growth rate of the instability for mode $m = 0$ is:

$$\frac{1}{\tau_0} = - \frac{eI_b c}{2Q\omega_0 E_0 \tau_L} \text{Re}(Z_{\perp}), \quad (59)$$

I_b being the bunch current.

For a positive chromaticity above transition $\omega_{\xi} > 0$, the bunch spectrum is shifted to the right by ω_{ξ} — Fig. 25. It is clear from Fig. 25 that a slightly positive value of ω_{ξ} is sufficient to stabilize the dipole mode $m = 0$ as the beam sees more impedance in positive frequency than in negative one. The higher modes require a larger value of ω_{ξ} for achieving stability.

In the case of space charge impedance $iZ_{\perp}(p)$ is real and constant. The coherent frequency shift is real and the motion is stable. Resistance is needed to drive instability.

In the case of very narrow parasitic high Q modes in RF resonators, the motion is driven by a single line at $(p + Q)\omega_0 + m\omega_s$, $p = -\infty, \dots, +\infty$. The imaginary part of the coherent frequency that determines the stability of the motion, is proportional to the resistance:

$$\text{Im}(\omega_c) \sim I \cdot \text{Re}(Z_{\perp}(p)). \quad (60)$$

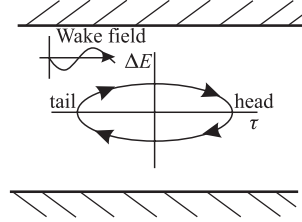


Fig. 23. Head-tail instability

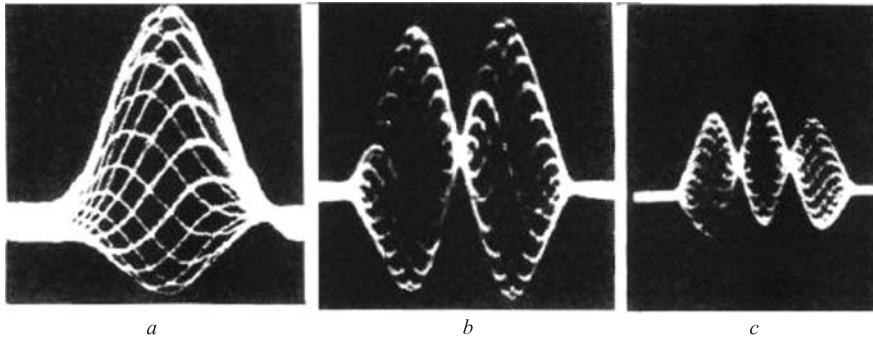


Fig. 24. The first three head-tail modes measured at PSB, a — — — $m = 0$, b — — — $m = 1$ and c — — — $m = 2$ modes

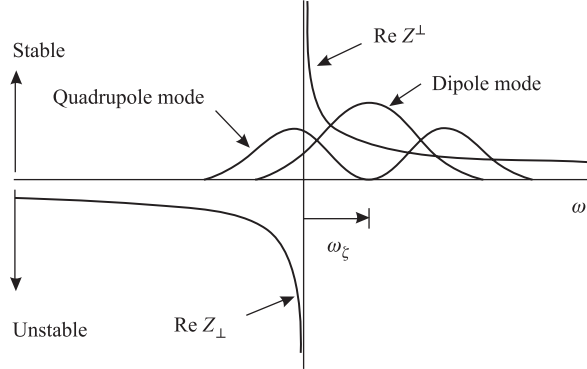


Fig. 25. Stabilization of resistive-wall head-tail instability by chromaticity

For instability to occur the negative resistance (negative frequency or $p < 0$) is needed. A positive value of ω_ξ is necessary to stabilize the motion.

If there is no single bunch but M , equally spaced bunches are present, and the couple-bunch modes can be driven. Similar to the longitudinal case the couple-bunch mode number « n » is introduced, $n = 0, 1, \dots, (M - 1)$. This index determines the phase shift between the coherent perturbations in two successive bunches. This phase shift is equal to $2\pi n/M$. Now the spectrum is a line spectrum at frequencies:

$$\omega = (n + pM + Q)\omega_0 + m\omega_s + \Delta\omega_{cm}. \quad (61)$$

4. STEPS AGAINST COHERENT INSTABILITIES

A careful design of the circular accelerator is usually sufficient to avoid the coherent instabilities. The vacuum chamber must be as smooth as possible. All the remained changes of the vacuum chamber cross section must be systematically shielded.

In electron/positron machines, a natural damping mechanism is due to the synchrotron radiation. To suppress the instability, the radiation damping time must be shorter than the instability growth time. The higher order modes (HOMs) in the accelerating resonators are the main source of concern in these accelerators. The HOMs are reduced by a special design of RF cavities.

In hadron machines, the Landau damping mechanism is usually sufficient to suppress the instability. At present, feedback systems are used in the modern accelerators with high intensity beams.

Appendix. Impedances and wake functions —[B3]

General Remarks and Notations:		
<p>W'_m denotes mth azimuthal longitudinal wake function as a function of distance z for $z < 0$. When $z > 0$, $W'_m(z) = 0$ and $W'_m(0) = \lim_{z \rightarrow 0^-} W'_m(z)$. Similar for transverse wake W_m.</p> <p>The mth azimuthal longitudinal impedance $Z_m^\parallel(\omega) = \int e^{-i\omega z/v} W'_m(z) dz/v$ is related to the transverse impedance of the same azimuthal $Z_m^\perp(\omega) = \int e^{-i\omega z/v} W_m^\perp(z) idz/(\beta v)$ by $Z_m^\parallel = (\omega/c)Z_m^\perp$ (valid when $m \neq 0$). In many cases, $\beta = v/c$ has been set to 1.</p> <p>Unless otherwise stated, round beam pipe of radius b is assumed. $C = 2\pi R$ is the ring circumference and n is the revolution harmonic. $Z_0 \approx 377 \Omega$ is the free-space impedance. ϵ_0 and μ_0 are the free-space dielectric constant and magnetic permeability.</p>		
Description	Impedances	Wakes
Space-charge: [1] beam radius a in a length L of perfectly conducting beam pipe of radius b .	$\frac{Z_0^\parallel}{n} = i \frac{Z_0 L}{2C\beta\gamma^2} \left[1 + 2 \ln \frac{b}{a} \right]$ $Z_{m \neq 0}^\perp = i \frac{Z_0 L}{2\pi\beta^2\gamma^2 m} \left[\frac{1}{a^{2m}} - \frac{1}{b^{2m}} \right]$	$W'_0 = \frac{Z_0 c L}{4\pi\gamma^2} \left[1 + 2 \ln \frac{b}{a} \right] \delta'(z)$ $W_{m \neq 0} = \frac{Z_0 c L}{2\pi\gamma^2 m} \left[\frac{1}{a^{2m}} - \frac{1}{b^{2m}} \right] \delta(z)$
Resistive Wall: [1] pipe length L , wall thickness t , conductivity σ_c , skin depth δ_{skin} .	$\frac{Z_m^\parallel}{L} = \frac{\omega}{c} \frac{Z_m^\perp}{L} = \frac{Z_0 c / (\pi b^{2m})}{[1 + \text{sgn}(\omega)i](1 + \delta_{m0})bc \sqrt{\frac{\sigma_c Z_0 c}{2 \omega } - \frac{ib^2\omega}{m+1} + \frac{imc^2}{\omega}}}$ $t \gg \delta_{\text{skin}} = \sqrt{2c/(\omega \sigma_c)}, \quad \omega \gg c\chi/b, \quad \chi = 1/(Z_0\sigma_c b)$	
For $t \gg \delta_{\text{skin}}$ and $b/\chi \gg z \approx c/ \omega \gg b\chi^{1/3}$.	$Z_m^\parallel = \frac{\omega}{c} Z_m^\perp$ $Z_m^\parallel = \frac{1 - \text{sgn}(\omega)i}{1 + \delta_{0m}} \frac{L}{\pi\sigma_c \delta_{\text{skin}} b^{2m+1}}$	$W_m = -\frac{c}{\pi b^{2m+1}(1 + \delta_{m0})} \sqrt{\frac{Z_0}{\pi\sigma_c}} \frac{L}{ z ^{1/2}}$ $W'_m = -\frac{c}{2\pi b^{2m+1}(1 + \delta_{m0})} \sqrt{\frac{Z_0}{\pi\sigma_c}} \frac{L}{ z ^{3/2}}$
For $t \ll \delta_{\text{skin}}$ or very low freq., and $b/\chi \gg z \approx c/ \omega \gg \sqrt{bt}$.	$\frac{Z_0^\parallel}{L} = -\frac{iZ_0 t \omega}{2\pi b c}, \quad \frac{Z_1^\perp}{L} = -\frac{iZ_0 t}{\pi b^3}$	$\frac{W'_0}{L} = -\frac{Z_0 t c}{2\pi b} \delta'(z), \quad \frac{W_1}{L} = -\frac{Z_0 t c}{\pi b^3} \delta(z)$
A pair of strip-line BPM's: [2] length L , angle each subtending to pipe axis ϕ_0 , forming transmission lines of characteristic impedance Z_c with pipe.	$Z_0^\parallel = 2Z_c \left[\frac{\phi_0}{2\pi} \right]^2 \left[2 \sin^2 \frac{\omega L}{c} - i \sin \frac{2\omega L}{c} \right]$ $Z_1^\perp = \left[\frac{Z_0^\parallel}{\omega} \right]_{\text{pair}} \frac{c}{b^2} \left[\frac{4}{\phi_0} \right]^2 \sin^2 \frac{\phi_0}{2}$	$W'_0 = 2Z_c c \left[\frac{\phi_0}{2\pi} \right]^2 [\delta(z) - \delta(z+2L)]$ $W_1 = \frac{8Z_c c}{\pi^2 b^2} \sin^2 \frac{\phi_0}{2} [H(z) - H(z+2L)]$
The strip-lines are assumed to terminate with impedance Z_c at the up-stream end.		
Heifets inductive impedance: [3] low freq. pure inductance \mathcal{L} . Z_0^\parallel rolls off as $\omega^{-1/2}$.	$Z_0^\parallel = -\frac{i\omega\mathcal{L}}{(1 - i\omega a/c)^{3/2}}$ $\rightarrow -i\omega\mathcal{L} \text{ as } a \rightarrow 0$	$W'_0 = \frac{c^2\mathcal{L}}{a\sqrt{\pi a z}} \left[1 + \frac{2z}{a} \right] e^{z/a}$ $\rightarrow c^2\mathcal{L}\delta'(z) \text{ as } a \rightarrow 0$
Pill-box cavity at low freq.: length g , radial depth $h + b$, where $g \leq h \ll b$ [6].	$Z_0^\parallel = -i \frac{\omega Z_0}{2\pi c b} \left[gh - \frac{g^2}{2\pi} \right]$ $Z_1^\perp = -i \frac{Z_0}{\pi b^3} \left[gh - \frac{g^2}{2\pi} \right]$	$W'_0 = -\frac{Z_0 c}{2\pi b} \left[gh - \frac{g^2}{2\pi} \right] \delta'(z)$ $W_1 = -\frac{Z_0 c}{\pi b^3} \left[gh - \frac{g^2}{2\pi} \right] \delta(z)$

Description	Impedances	Wakes
Pill-box cavity at low freq.: length g , radial depth $h + b$, where $h \ll g \ll b$ [6].	$Z_0^{\parallel} = -i \frac{\omega Z_0 h^2}{\pi^2 c b} \left[\ln \frac{2\pi g}{h} + \frac{1}{2} \right]$ $Z_1^{\perp} = -i \frac{2Z_0 h^2}{\pi^2 b^3} \left[\ln \frac{2\pi g}{h} + \frac{1}{2} \right]$	$W_0' = -\frac{Z_0 c h^2}{\pi^2 b} \left[\ln \frac{2\pi g}{h} + \frac{1}{2} \right] \delta'(z)$ $W_1 = -\frac{2Z_0 c h^2}{\pi^2 b^3} \left[\ln \frac{2\pi g}{h} + \frac{1}{2} \right] \delta(z)$
Pill-box cavity: length g , radial depth d . At freq. $\omega \gg c/b$, diffraction model applies [1].	$Z_m^{\parallel} = \frac{[1 + \text{sgn}(\omega)i] Z_0}{(1 + \delta_{m0}) \pi^{3/2} b^{2m+1}} \sqrt{\frac{cg}{ \omega }}$ $Z_m^{\perp} = \frac{\omega}{c} Z_m^{\parallel}$	$W_m = -\frac{2Z_0 c \sqrt{2g}}{(1 + \delta_{m0}) \pi^{2} b^{2m+1}} z ^{1/2}$ $W_m' = \frac{Z_0 c \sqrt{2g}}{(1 + \delta_{m0}) \pi^{2} b^{2m+1}} z ^{-1/2}$
Optical model: [7] A series of cavities of periodic length L . Each cavity has width g , high Q resonances of freq. $\omega_n/(2\pi)$ and loss factor $k_n^{(m)}$ for azimuthal mode m .	$\text{Re} Z_m^{\parallel} = \sum_{n=1}^N \pi k_n^{(m)} \delta(\omega - \omega_n) + \frac{2\pi C_{\text{sv}} G(\bar{\nu}) F(\nu)}{(1 + \delta_{m0}) b^{2m}} H(\omega - \omega_N)$ $W_m' = \sum_{n=1}^N 2k_n^{(m)} \cos \frac{\omega_n z}{c} + \frac{2C_{\text{sv}} G(\bar{\nu})}{(1 + \delta_{m0}) b^{2m}} \int_{\omega_N}^{\infty} d\omega F(\nu) \cos \frac{\omega z}{c}$ <p>where $C_{\text{sv}} = 2Z_0 J_{m1}^2 / (\pi^2 \zeta^2 \beta) \approx 650 \Omega$ for $m = 0$ and 1650Ω for $m = 1$, J_{m1} is first zero of Bessel function J_m, $\zeta = 0.8237$.</p> $G(\bar{\nu}) = \bar{\nu}^2 K_1^2(\bar{\nu}), \quad F(\nu) = \frac{\sqrt{\nu+1}}{(\nu+2\sqrt{\nu+2})^2}, \quad \bar{\nu} = \frac{\omega b}{\beta \gamma c}, \quad \nu = \frac{\omega}{\omega_{\text{sv}}} = \frac{4b^2 \omega}{\zeta^2 c \sqrt{g} L}$	
Formulas for computation of W_m' . $\text{erfc}(x)$ is the complementary error function.	$\int_{\tilde{\omega}}^{\infty} d\omega F(\nu) \cos \frac{\omega z}{c} = \omega_{\text{sv}} \tilde{F}_0(z/c) - \int_0^{\tilde{\omega}} d\omega F(\nu) \cos \frac{\omega z}{c}$ $\tilde{F}_0(x) = \int_0^{\infty} d\omega F(\nu) \cos \omega x = \frac{\pi}{4} (1 + 4x) e^{2x} \text{erfc}(\sqrt{2x}) - \sqrt{\frac{\pi x}{2}}$	
Resonator model for the m th azimuthal, with shunt imp. $R_s^{(m)}$, resonant freq. $\omega_r/(2\pi)$, quality factor Q [1].	$Z_m^{\parallel} = \frac{R_s^{(m)}}{1 + iQ(\omega_r/\omega - \omega/\omega_r)}$ $Z_m^{\perp} = \frac{c}{\omega} \frac{R_s^{(m)}}{1 + iQ(\omega_r/\omega - \omega/\omega_r)}$	$W_m = \frac{R_s^{(m)} c \omega_r}{Q \tilde{\omega}_r} e^{\alpha z/c} \sin \frac{\tilde{\omega}_r z}{c}$ <p>where $\alpha = \omega_r/(2Q)$ $\tilde{\omega}_r = \sqrt{ \omega_r^2 - \alpha^2 }$</p>
Res. freq. $\omega_{mnp}/(2\pi)$ and shunt impedance $(R_s)_{mnp}$ of a pill-box cavity for n th radial and p th longitudinal modes. Radial depth d and length g . x_{mn} is n th zero of Bessel function J_m [8].	$\frac{\omega_{mnp}^2}{c^2} = \frac{x_{mn}^2}{d^2} + \frac{p^2 \pi^2}{g^2}$ $\left[\frac{R_s}{Q} \right]_{0np} = \frac{Z_0}{x_{0n}^2 J_0^2(x_{0n})} \frac{8c}{\pi g \omega_{0np}} \begin{cases} \sin^2 \frac{g\omega_{0np}}{2\beta c} \times \frac{1}{1 + \delta_{0p}} & p \text{ even} \\ \cos^2 \frac{g\omega_{0np}}{2\beta c} & p \text{ odd} \end{cases}$ $\left[\frac{R_s}{Q} \right]_{1np} = \frac{Z_0}{J_1^2(x_{1n})} \frac{2c^2}{\pi g d^2 \omega_{1np}^2} \begin{cases} \sin^2 \frac{g\omega_{1np}}{2\beta c} & p \neq 1 \text{ and even} \\ \cos^2 \frac{g\omega_{1np}}{2\beta c} & p \text{ odd} \end{cases}$	

Description	Impedances	Wakes
Low-freq. response of a pill-box cavity: [4] length g , radial depth d . When $g \gg 2(d-b)$, replace g by $(d-b)$. Here, $S = d/b$.	$\frac{Z_0^{\parallel}}{n} = -i \frac{Z_0 g}{2\pi R} \ln S$ $Z_1^{\perp} = -i \frac{Z_0 g}{\pi b^2} \frac{S^2 - 1}{S^2 + 1}$	$W'_0 = -\frac{Z_0 c g}{2\pi} \ln S \delta'(z)$ $W_1 = -\frac{Z_0 c g}{\pi b^2} \frac{S^2 - 1}{S^2 + 1} \delta(z)$
	Effect will be one half for a step in the beam pipe from radius b to radius d , or vice versa, when $g \gg 2(d-b)$.	
Iris of half elliptical cross section at low freq.: width $2a$, maximum protruding length h [5].	$Z_0^{\parallel} = -i \frac{\omega Z_0 h^2}{4cb}$ $Z_1^{\perp} = -i \frac{Z_0 h^2}{2b^3}$	$W'_0 = -\frac{Z_0 c h^2}{4b} \delta'(z)$ $W_1 = -\frac{Z_0 c h^2}{2b^3} \delta(z)$
Pipe transition at low freq.: tapering angle θ , transition height h . γ is Euler's constant and ψ is the psi-function [6].	$Z_0^{\parallel} = \frac{\omega b^2 Z_1^{\perp}}{2c} = -i \frac{\omega Z_0 h^2}{2\pi^2 c b} \left\{ \ln \left[\frac{b\theta}{h} - 2\theta \cot \theta \right] + \frac{3}{2} - \gamma - \psi \left(\frac{\theta}{\pi} \right) - \frac{\pi}{2} \cot \theta - \frac{\pi}{2\theta} \right\}$ $W'_0 = -\left \frac{Z_0^{\parallel}}{\omega} \right c^2 \delta'(z), \quad W_1 = - Z_1^{\perp} c \delta(z), \quad h \cot \theta \ll b$	
Pipe transition at low frequencies with transition height $h \ll b$ [6].	$Z_0^{\parallel} = \frac{\omega b^2}{2c} Z_1^{\perp} = -i \frac{\omega Z_0 h^2}{2\pi^2 c b} \left(\ln \frac{2\pi b}{h} + \frac{1}{2} \right)$ $W'_0 = -\left \frac{Z_0^{\parallel}}{\omega} \right c^2 \delta'(z), \quad W_1 = - Z_1^{\perp} c \delta(z)$	
Kicker with window-frame magnet [9]: width a , height b , length L , beam offset x_0 horizontally, and all image current carried by conducting current plates.	$Z_0^{\parallel} = \frac{\omega^2 \mu_0^2 L^2 x_0^2}{4a^2 Z_k}$ $Z_1^{\perp} = \frac{c \omega \mu_0^2 L^2}{4a^2 Z_k}$	$W'_0 = -\frac{c^3 \mu_0^2 L^2 x_0^2}{4a^2 Z_k} \delta_0''(z)$ $W_1 = -\frac{c^3 \mu_0^2 L^2}{4a^2 Z_k} \delta'(z)$
	$Z_k = -i\omega\mathcal{L} + Z_g$ with $\mathcal{L} \approx \mu_0 b L / a$ the inductance of the windings and Z_g the impedance of the generator and the cable. If the kicker is of C-type magnet, x_0 in Z_0^{\parallel} should be replaced by $(x_0 + b)$.	
Traveling-wave kicker with characteristic impedance Z_c for the cable, and a window magnet of width a , height b , and length L [9].	$Z_0^{\parallel} = \frac{Z_c}{4} \left[2 \sin^2 \frac{\theta}{2} - i(\theta - \sin \theta) \right], \quad Z_1^{\perp} = \frac{Z_c L}{4ab} \left[\frac{1 - \cos \theta}{\theta} - i \left(1 - \frac{\sin \theta}{\theta} \right) \right]$ $W'_0 = \frac{Z_c c}{4} \left[\delta(z) - \delta \left(z - \frac{Lc}{v} \right) - \frac{Lc}{v} \delta'(z) \right]$ $W_1 = \frac{Z_c v}{4ab} \left[H(z) - H \left(z - \frac{Lc}{v} \right) - \frac{Lc}{v} \delta(z) \right]$	$\theta = \omega L / v$ denotes the electrical length of the kicker windings and $v = Z_c a c / (Z_0 b)$ is the matched transmission-line phase velocity of the capacitance-loaded windings.
Bethe's electric and magnetic moments of a hole of radius a in beam pipe wall [10].	Electric and magnetic dipole moments when wavelength $\gg a$: $\vec{d} = -\frac{2\epsilon_0}{3} a^3 \vec{E}$, $\vec{m} = -\frac{4}{3\mu_0} a^3 \vec{B}$ \vec{E} and \vec{B} are electric and magnetic flux density at hole when hole is absent. This is a diffraction solution for a thin-wall pipe.	

Description	Impedances	Wakes
Small obstacle [5, 11] on beam pipe, size \ll pipe radius, freq. below cutoff. α_e and α_m are electric polarizability and magnetic susceptibility of the obstacle.	$Z_0^{\parallel} = -i \frac{\omega Z_0}{c} \frac{\alpha_e + \alpha_m}{4\pi^2 b^2}$ $Z_1^{\perp} = -i \frac{Z_0(\alpha_e + \alpha_m)}{\pi^2 b^4} \cos \Delta\varphi$	$W_0' = -Z_0 c \frac{\alpha_e + \alpha_m}{4\pi^2 b^2} \delta'(z)$ $W_1 = -Z_0 c \frac{\alpha_e + \alpha_m}{\pi^2 b^4} \cos \Delta\varphi \delta(z)$
	$\Delta\varphi$ is the azimuthal angle between the obstacle and the direction concerning Z_1^{\perp} and W_1 .	
Polarizabilities for various geometry: beam pipe radius is b and wall thickness is t .		
Elliptical hole: major and minor radii are a and d . $K(m)$ and $E(m)$ are complete elliptical functions of the first and second kind, with $m = 1 - m_1$ and $m_1 = (d/a)^2$. For long ellipse \perp beam, major axis $a \ll b$, beam pipe radius, because the curvature of the beam pipe has been neglected here [12].	$\alpha_e + \alpha_m = \begin{cases} \frac{\pi a^3 m_1^2 [K(m) - E(m)]}{3E(m)[E(m) - m_1 K(m)]} & \xrightarrow{m \rightarrow 1} \\ \frac{\pi a^3 [E(m) - m_1 K(m)]}{3[K(m) - E(m)]} & \text{long ellipse} \end{cases}$ $\alpha_e + \alpha_m \xrightarrow{\text{circular}} \frac{2a^3}{3} \quad \text{circular hole } a = d \ll b$	$\begin{cases} \frac{\pi d^4 [\ln(4a/d) - 1]}{3a} & \parallel \text{ beam } d \ll b \\ \frac{\pi a^3}{3 [\ln(4a/d) - 1]} & \perp \text{ beam } a \ll b \end{cases}$
	Above are for $t \ll a$, $\times 0.56$ (circular) or $\times 0.59$ (long ellipse) when $t \geq a$. For higher frequency correction, add to $\alpha_e + \alpha_m$ the extra term,	
	$+ \frac{2\pi a^3}{3} \left[\frac{11\omega^2 a^2}{30c^2} \right] \text{circular, } \begin{cases} -\frac{\pi a d^2}{3} \left[\frac{\omega^2 a^2}{5c^2} \right] & \parallel \text{ beam long ellipse} \\ +\frac{2\pi a^3}{3} \left[\frac{2\omega^2 a^2}{5c^2 [\ln(4a/d) - 1]} \right] & \perp \text{ beam long ellipse} \end{cases}$	
Rectangular slot: length L , width w .	$\alpha_e + \alpha_m = w^3(0.1814 - 0.0344w/L) \quad t \ll a, \quad \times 0.59 \text{ when } t \geq a$	
Rounded-end slot: length L , width w .	$\alpha_e + \alpha_m = w^3(0.1334 - 0.0500w/L) \quad t \ll a, \quad \times 0.59 \text{ when } t \geq a$	
Annular-ring-shaped cut: inner and outer radii a and $d = a + w$ with $w \ll d$.	$\alpha_e + \alpha_m = \frac{\pi^2 d^2 a}{2 \ln(32d/w) - 4} - \frac{\pi^2 w^2 (a + d)}{16} \quad t \ll d$ $\alpha_e + \alpha_m = \pi d^2 w - \frac{1}{2} w^2 (a + d) \quad t \geq d$	
Half ellipsoidal protrusion with semi-axes h radially, a longitudinally, and d azimuthally. ${}_2F_1$ is the hypergeometric function.	$\alpha_e + \alpha_m = 2\pi a h d \left[\frac{1}{I_b} + \frac{1}{I_c - 3} \right]$ $I_b = {}_2F_1\left(1, 1; \frac{5}{2}; 1 - \frac{h^2}{a^2}\right), \quad I_c = {}_2F_1\left(1, \frac{1}{2}; \frac{5}{2}; 1 - \frac{a^2}{d^2}\right), \quad \text{if } a = d$ $\alpha_e + \alpha_m = \pi a^3 \quad \text{if } a = d = h, \quad \frac{2\pi h^3}{3 [\ln(2h/a) - 1]} \quad \text{if } a = d \ll h$ $\alpha_e + \alpha_m = \frac{8h^3}{3} \left[1 + \left(\frac{4}{\pi} - \frac{\pi}{4} \right) \frac{a}{h} \right] \quad \text{if } a \ll h = d$ $\alpha_e + \alpha_m = \frac{8\pi h^4}{3a} \left[\ln \frac{2a}{h} - 1 \right] \quad \text{if } a \gg h = d$	

<p>Array of pill-boxes, box spacing L, each with gap width g, beam pipe radius b. Gluckstern-Yokoyama-Bane formula [15] at high freq. to order $(kg)^{-1}$:</p>	<p>For each cavity of length L with $k = \omega/c$,</p> $Z_0^{\parallel} = \frac{iZ_0L}{\pi kb^2} \left\{ 1 + [1 + i \operatorname{sgn}(k)] \frac{\alpha L}{b} \sqrt{\frac{\pi}{ k g}} \right\}^{-1}$ <p>with $k = \omega/c$. $\alpha = 1$ when $g/L \ll 1$ and $\alpha = \alpha_1 = 0.4648$ when $g/L = 1$, the limiting case of infinitely thin irises. In general, with $\Upsilon = g/L$, $\alpha(\Upsilon) = 1 - \alpha_1 \Upsilon^{1/2} - (1 - 2\alpha_1)\Upsilon + \mathcal{O}(\Upsilon^{3/2})$.</p>
<p>The above pill-box array with radial depth d generates a single-frequency resonance impedance at $\omega_r = c \left(\frac{2L}{bgd} \right)^{1/2}$ [16, 17].</p>	$Z_0^{\parallel} = \frac{Z_0cL}{2\pi b^2} \sum_{\omega'=\pm\omega_r} \left[\pi\delta(\omega-\omega') + \frac{i}{\omega-\omega'} \right]$ $Z_1^{\perp} = \frac{2cL}{b^2\omega} Z_0^{\parallel}$ $W_0'(z) = \frac{Z_0cL}{\pi b^2} \cos \frac{\omega_r z}{c}$ $W_1(z) = \frac{2Z_0L}{\pi b^4\omega_r} \sin \frac{\omega_r z}{c}$ <p>The corresponding resonator per pill box has $\frac{R_s^{(0)}\omega_r}{Q} = \frac{Z_0cL}{\pi b^2}$.</p>
<p>Smooth toroidal b and $R = \frac{1}{2}(a+b)$. As the Lorentz factor $\gamma \rightarrow \infty$, (ultra-relativistic beam), a <u>curvature contribution</u> remains for the longitudinal impedance [18].</p>	<p>Valid from zero frequency up to just below synchronous resonant modes, i.e., $0 < \nu < \sqrt{R/h}$ with $\nu = \omega h/c$,</p> $\frac{Z_0^{\parallel}}{n} = iZ_0 \left(\frac{h}{\pi R} \right)^2 \left\{ \left[1 - e^{-2\pi(b-R)/h} - e^{-2\pi(R-a)/h} \right] \left[1 - 3 \left(\frac{\nu}{\pi} \right)^2 \right] + 0.05179 - 0.01355 \left(\frac{\nu}{\pi} \right)^2 \right\} + \rho$ $\approx iZ_0 \left(\frac{h}{\pi R} \right)^2 \left[A - 3B \left(\frac{\nu}{\pi} \right)^2 \right]$ <p>where ρ is quadratic in ν. As $(b-a)/h$ increases, ρ vanishes exponentially and $A \approx B \approx 1$. In general, $A/B \approx 1$ implying $\operatorname{Im}Z_0^{\parallel}$ changes sign (a node) near $\nu = \pi/\sqrt{3}$.</p>
<p>Rf cage: beam of radius a surrounded by a cylindrical cage or array of N wires of radius ρ_w, length L at radial distance r_w from beam center. Wire filling factor is $f_w = N\rho_w/(\pi r_w)$. Formulas are valid at low frequencies, $0 < n < R/r_w$ and $N \gg 1$.</p>	$\frac{Z_0^{\parallel}}{n} = \frac{iZ_0L}{4\pi R\beta\gamma^2} \left[1 + 2 \ln \frac{r_w}{a} + C_{\parallel} \right], \quad Z_1^{\perp} = \frac{iZ_0L}{2\pi\beta^2\gamma^2} \left[\frac{1}{a^2} - \frac{1 - C_{\perp}}{r_w^2} \right]$ <p>Without metallic beam pipe outside wire array or cage [19],</p> $C_{\parallel} = -\frac{2 \ln(nr_w/R) \ln(\pi f_w)}{N \ln(nr_w/R) + \ln(\pi f_w)}, \quad C_{\perp} = -\frac{2 \ln(\pi f_w)}{N - 2 \ln(\pi f_w)}$ <p>With infinitely conducting metallic beam pipe, radius $b > r_w$ [20],</p> $C_{\parallel} = 2 \ln \frac{b}{r_w} - \frac{2N[\ln(b/r_w)]^2}{N \ln(b/r_w) - \ln(\pi f_w) + \ln[1 - (r_w/b)^{2N}]}$ $C_{\perp} = \frac{[1 - (r_w/b)^2][(r_w/b)^2 + (b/r_w)^2] \{ \ln[1 - (r_w/b)^{2N}] - 2 \ln(\pi f_w) \}}{N[1 - (r_w/b)^2] + [(r_w/b)^2 + (b/r_w)^2] \ln[1 - (r_w/b)^{2N}] - 2 \ln(\pi f_w)}$ <p>A ceramic layer between the wires and metallic beam pipe has negligible effect on the impedances.</p>

<p>Wall roughness [13] 1-D axisymmetric bump, $h(z)$ or 2-D bump $h(z, \theta)$. Valid for low frequency $k = \omega/c \ll (\text{bump length or width})^{-1}$, $h \ll b$, pipe radius, and $\nabla h \ll 1$.</p>	<p>1-D: $Z_0^{\parallel} = -\frac{2ikZ_0}{b} \int_0^{\infty} \kappa \bar{h}(\kappa) ^2 d\kappa$ with spectrum $\bar{h}(k) = \frac{1}{2\pi} \int_{-\infty}^{\infty} h(z) e^{-ikz} dz$ 2-D: $Z_0^{\parallel} = -\frac{4ikZ_0}{b} \sum_{m=-\infty}^{\infty} \int_{-\infty}^{\infty} \frac{\kappa^2}{\sqrt{\kappa^2 + m^2/b^2}} \bar{h}_m(\kappa) ^2 d\kappa$ with spectrum $\bar{h}_m(k) = \frac{1}{(2\pi)^2} \int_0^{2\pi} d\theta \int_{-\infty}^{\infty} dz h(z, \theta) e^{-ikz - im\theta}$</p>
<p>Heifets and Kheifets formulas for tapered steps and tapered cavity at high frequencies [14].</p>	
<p>Taper in from radius h to b ($< h$), out from radius b to h; tapering angle α. Tapering inefficient for a bunch of rms length σ, if $2(h-b) \tan \alpha \gg \sigma$. All formulas here and below are valid for <i>positive</i> $k = \omega/c$ only.</p>	<p>$\text{Re} Z_0^{\parallel} = \pm \frac{Z_0}{2\pi} \ln \frac{h}{b} + (Z_0^{\parallel})_{\text{step}}$, $\text{Re} Z_1^{\perp} = \pm \frac{Z_0 b}{4\pi} \left(\frac{1}{b^2} - \frac{1}{h^2} \right) + (Z_1^{\perp})_{\text{step}}$ $\begin{cases} +\text{in} \\ -\text{out} \end{cases}$ $(Z_0^{\parallel})_{\text{step}} = \frac{Z_0}{2\pi} \ln \frac{h}{b}$, $\tan \alpha > \frac{h-b}{kb^2}$, $(Z_0^{\parallel})_{\text{step}} = \frac{Z_0}{4} kb \tan \alpha$, $\tan \alpha \ll \frac{1}{kb}$ $(Z_1^{\perp})_{\text{step}} = \frac{Z_0}{4\pi b} \left[1 - \frac{1}{(1+kb)^2} {}_2F_1 \left(1, \frac{3}{2}, 3, \frac{4bh}{(b+h)^2} \right) \right]$, $\tan \alpha > \frac{h-b}{kb^2}$, $kb \gg 1$ $(Z_1^{\perp})_{\text{step}} = \frac{Z_0 b}{4\pi} \left(\frac{1}{b^2} - \frac{1}{h^2} \right)$, $\tan \alpha > \frac{h-b}{kb^2}$, $kb \gg 1$, $h \gg b$ $(Z_1^{\perp})_{\text{step}} = \frac{Z_0}{16b} (kb)^3 \tan \alpha$, $\tan \alpha \ll \frac{1}{kb}$</p>
<p>Pill-box cavity: total length g, radial depth h without taper. Tapering angle α on both sides, $g \gg h$.</p>	<p>$Z_0^{\parallel} = \begin{cases} \frac{(1+i)Z_0}{2\pi b} \sqrt{\frac{g}{k\pi}} & g \ll kb^2 \\ -i \frac{Z_0}{\pi} \ln \frac{h}{b} & g \gg kb^2 \end{cases}$ $\text{Re} Z_0^{\parallel} = 2 (Z_0^{\parallel})_{\text{step}}$, $\text{Re} Z_0^{\perp} = 2 (Z_0^{\perp})_{\text{step}}$ as given above</p>

REFERENCES

1. Vaccaro V. G. CERN preprint No. ISR-RF/66-35. 1966.
2. Zotter B., Sacherer F. Proceedings of International School on Particle Accelerators, Erice, 1976. P. 175.
3. Sessler A. M., Vaccaro V. G. CERN preprint No. 672. 1987.
4. Palumbo L., Vaccaro V. G. Wake fields, Impedances and Green's function // CERN Accelerator School, Advanced Accelerator Physics. 1985. V. 1. CERN 87-03. 1987. P. 341–369.
5. Zotter B. Electromagnetic Fields, Impedances and Wakes // AIP Conference Proceedings. Physics of Particle Accelerators. N.Y., 1987. No. 1. P. 663–696.
6. Laclare J. L. Coasting Beam Longitudinal Coherent Instabilities // CERN Accelerator School, Fifth General Accelerator Physics Course. 1992. P. 349–384.

7. *Laclare J. L.* Coasting Beam Transverse Coherent Instabilities // CERN Accelerator School, Fifth General Accelerators Physics Course. 1992. P. 385–408.
8. *Moth M., Weng W. T.* Hadron-Hadron Colliders // AIP Conference Proceedings. Physics of High Energy Particle Accelerators. N. Y., 1983. No. 105. P. 124–280.
9. *Wang J. M.* Modes of Storage Ring Coherent Instabilities // AIP Conference Proceedings. Physics of Particle Accelerators. N. Y., 1987. No. 153. P. 697–788.
10. *Keil E., Schnell W.* CERN preprint No. ISR-TH-RF/69-48. 1969.
11. *Hubner K., Vaccaro V. G.* CERN preprint No. ISR-TH/70-44. 1970.
12. *Chao A. W.* Coherent Instabilities of a Relativistic Bunched Beam // AIP Conference Proceedings. Physics of High Energy Particle Accelerators. N. Y., 1983. No. 105. P. 353–523.
13. *Laclare J. L.* Bunched Beam Coherent Instabilities // CERN Accelerator School. Advanced Accelerator Physics. 1985. P. 264–326.
14. *Sacherer F. J.* A Longitudinal Stability Criterion for Bunched Beams // Proceedings of the Fifth Particle Accelerators Conference, San Francisco, 1973. P. 825–829.
15. *Sacherer F. J.* Bunch Lengthening and Microwave Instability // IEEE Trans. Nucl. Sci. 1977. V. NS-24, No. 3. P. 1393–1395.
16. *Pellegrini C.* Longitudinal Instabilities in Circular Accelerators and Storage Ring // IEEE Trans. Nucl. Sci. 1981. V. NS-28, No. 3. P. 2413–2419.
17. *Ruth R. D., Wang J. M.* Vertical Fast Blow-Up in a Single Bunch // IEEE Trans. Nucl. Sci. 1981. V. NS-28, No. 3. P. 2405–2407.
18. *Krinsky S., Wang J. M.* Longitudinal Instabilities of Long Gaussian Bunches // IEEE Trans. Nucl. Sci. 1983. V. NS-30, No. 4. P. 2495–2497.
19. *Boussard D.* CERN preprint No. LAB II/RF/INT/75-2. 1975.
20. *Hansen S., Hofmann A.* ISR Performance Report // CERN Int. Report No. ISR-GS/RF-AH/amb. 1976.
21. *Pellegrini C.* // Nuovo Cim. 1969. V. 64A. P. 477.
22. *Robinson K. W.* SLAC Storage Ring Summer Study, 1965 // Report SLAC-49. 1965. P. 69.

Received on December 10, 2009.

Редактор *Э. В. Ивашкевич*

Подписано в печать 19.03.2010.

Формат 60 × 90/16. Бумага офсетная. Печать офсетная.

Усл. печ. л. 1,75. Уч.-изд. л. 2,44. Тираж 270 экз. Заказ № 56934.

Издательский отдел Объединенного института ядерных исследований
141980, г. Дубна, Московская обл., ул. Жолио-Кюри, 6.

E-mail: publish@jinr.ru

www.jinr.ru/publish/